

Multi Receptive Field Network for Semantic Segmentation

Jianlong Yuan Zelu Deng Shu Wang Zhenbo Luo
 Samsung Research China Beijing

yj19122@163.com, zelu.deng@stu.uestc.edu.cn

s0913.wang@samsung.com, luozhenbo@tsinghua.org.cn

Abstract

Semantic segmentation is one of the key tasks in computer vision, which is to assign a category label to each pixel in an image. Despite significant progress achieved recently, most existing methods still suffer from two challenging issues: 1) the size of objects and stuff in an image can be very diverse, demanding for incorporating multi-scale features into the fully convolutional networks (FCNs); 2) the pixels close to or at the boundaries of object/stuff are hard to classify due to the intrinsic weakness of convolutional networks. To address the first issue, we propose a new Multi-Receptive Field Module (MRFM), explicitly taking multi-scale features into account. For the second issue, we design an edge-aware loss which is effective in distinguishing the boundaries of object/stuff. With these two designs, our Multi Receptive Field Network achieves new state-of-the-art results on two widely-used semantic segmentation benchmark datasets. Specifically, we achieve a mean IoU of 83.0% on the Cityscapes dataset and 88.4% mean IoU on the Pascal VOC2012 dataset.

1. Introduction

The task of semantic segmentation is one of the key technologies in visual understanding, which is widely used in object parsing, scene parsing, human body parsing and automatic driving, etc. The task is to predict each pixel in the image into a prescribed set of categories [3, 9, 23, 11, 14], which is a dense per-pixel prediction task. In recent years, compared with systems relying on hand-crafted features [16, 29, 18, 28, 13, 36], semantic segmentation methods based on deep FCN [25] have made tremendous progress, and these methods have achieved very impressive results on semantic segmentation benchmarks. Despite the success, FCNs still have two limitations.

First, the sizes of objects/stuff in images can be very diverse, making accurate prediction very challenging. In order to solve this problem, it is necessary to capture multi-scale features into FCNs. It is well known that multi-scale

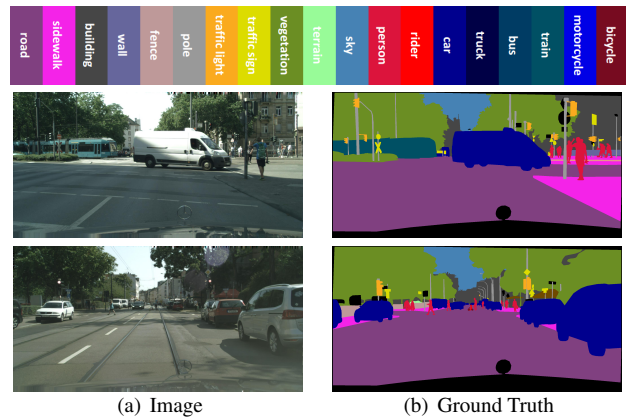


Figure 1. Illustration of challenging scenes in the Cityscapes dataset [9]. Various scales and indistinguishable boundaries of objects/stuff makes it challenging to accurately parse each pixel.

features benefit many computer vision tasks such as image classification, object detection and semantic segmentation. A straightforward approach is to resize the input image to different scales and input each copy to a share-parameter network. At some stage of the network, convolutional features are fused by concatenation or summation [22]. The second approach is to use skip connections to fuse features from different layers as introduced in ResNet [15]. DeeplabV3 [6] proposes the ASPP module, which applies several parallel atrous convolutions to obtain multi-scale receptive fields. The PSPNet [41] method proposes a PSP module, which applies multiple pooling with different sizes to obtain multi-scale features. These two methods are widely used and represent the current state-of-the-art methods. However, previous works haven't focused on how to acquire multi-scale receptive field in the backbone. Here we propose a new *multi-receptive field module (MRFM)*. Unlike previous works, we introduce the multi-receptive field module by re-designing the backbone work. Meanwhile, considering the trade-off between speed and performance, we also propose a light-weight version of MRFM, which does not introduce computation overhead for inference.

The second problem is that it is difficult to distinguish the

boundaries of objects/stuff. Recently, some works pay extra attention to the classification of pixels at edges, achieving improved results. DFN [37] combines the edge detection task with the semantic segmentation task. By observing the fact that edge pixels tend to be incorrectly classified, we design a new *edge aware loss*. The main idea is that during the training, a pixel close to or on the edge is assigned a weight which incurs a weighted penalty for the classifier.

Specially, our approach achieves state-of-the-art performance on the Cityscapes dataset [9] and the Pascal VOC2012 dataset [11]. Our main contributions are summarized as follows.

- We propose a multi-receptive field module (MRFM), which is crucial for improving prediction performance. Meanwhile, considering the trade-off between performance and inference efficiency, we design a lightweight MRFM.
- We design an edge-aware loss to separate the boundary more accurately. The loss function does not need additional annotated data, but can be computed only on existing semantic segmentation data.
- The proposed network achieves new state-of-the-art performance on the Cityscapes and Pascal VOC2012 dataset. In particular, we achieve an mIoU score of 83.0% on Cityscapes, and an mIoU score of 88.4% on the Pascal VOC2012 dataset.

1.1. Related Works

Models based on Fully Convolution Networks [25] have achieved high performance on several segmentation benchmarks [11, 9]. Here we review some works most relevant to ours, focusing on the issues of receptive fields and improving edge pixel classification.

Receptive Field: It is well known that the size of receptive fields is critically important for high-level computer vision tasks. In dense prediction tasks like semantic segmentation, depth estimation, it is crucial for each prediction pixel to have a receptive field that is sufficiently large such that context information can be considered for making a correct prediction. To enlarge the receptive field, the feature map’s output stride is set to 8, or 16 of the input size in semantic segmentation. On the other hand, as one has to upsample the output to the original input size, a large output stride may degrade the accuracy of per-pixel prediction. That is one of the reasons why multi-scale receptive field, corresponding to multi-scale features, can be beneficial for per-pixel prediction. Another interpretation is that, to make the network robust to a certain degree of invariance to translation, FCNs employ convolutions with stride and/or pooling for this purpose. However, this translation invariance is very harmful to accurately predict the labels

of pixels at the edge as a shift of several pixels may result in the same feature for pixel classification. This is dilemma. To use features from different levels of layers can partially alleviate this problem, which is essentially the same as using multiple different scales of features. In order to aggregate multi-scale context, the work of [38] employs a series of atrous convolution with increasing rates. Following [38], deeplabv2 [5] proposes a astrous spatial pyramid pooling (ASPP) which applies four parallel atrous convolution with different rates at the bottom of ResNet [15]. With the evolution of Deeplab architectures, ASPP forms several parallel atrous convolutions and an global average pooling structure, and all of operations contain batch normalization. ASPP has shown its success in extracting features of different scales. Besides, DenseASPP [35] proposes an improved ASPP which is inspired by DenseNet [17]. RefinNet [21] proposes an chained residual pooling which captures background context from a large image region. PSPNet [41] proposes a Spatial Pyramid Pooling (PSP) to extract feature maps with different sizes of pooling, then concatenates all the feature maps after upsampling. Notably, all of these modules are placed at the end of the backbone. We design a different approach that achieves multi-receptive field by interleaving in the backbone.

Objects/stuff Edge: In the traditional image segmentation task, many methods attempt to use edge or low-level information to improve performance. For the semantic segmentation method based on deep learning, the use of edges can be divided into two categories. The first one is using an Encoder-Decoder architecture that refines the final prediction with low-level features. Low-level features make the results sharper. For examples, SegNet [1] utilizes the saved pool indices to recover the reduced spatial information. Unet [26] uses different spatial information by skip connection. MSCI [20] aggregates features form different scales with two LSTM chains. The other is multi-task that shares parameters for both semantic segmentation and edge detection, such as DFN [37]. The work of [44] shows that an auxiliary task (the edge agreement head) leads to faster training of the mask segmentation task.

2. Methods

In this section, we introduce our proposed *Multi-Receptive Field module* in detail first. Then, we present the *Edge Aware Loss*. Finally, we describe the complete network architecture.

2.1. Multi-Receptive Field Module

Most of the methods capture multi-receptive field by modifying the structure at the end of the network [5, 41, 35]. However, previous works have not pay much attention on how to design a backbone to capture multi-receptive field. Therefore, we propose the *multi receptive field module*

(*MRFM*) by redesigning the backbone, illustrated in the Figure 2.

Multi-Receptive Field Module (MRFM): Generally, the backbone has a basic module, such as bottleneck in ResNet [15], the basic module in Xception [8]. Take Xception for example. The basic module is composed of three depthwise convolution, one skip connection or skip connection with 1×1 convolution. It’s easy to understand that the basic module only captures single scale receptive field. Therefore, it is difficult to segment multi-scale objects accurately. So, we propose a *multi-receptive field module (MRFM)* that can simply replace any basic module, illustrated in the Figure 2. MRFM is composed of two paths with different receptive field. One path of MRFM is the same as the basic module, which called standard path. The other path, called atrous path, has the same structure as the basic module, but the convolution method is replaced by atrous convolution. In order to adaptively choose which receptive field is suitable, the output of each path is added by weights. In particular, two weights are normalized. To sum up, MRFM is explained by Equation 1, where $f_1(*)$ denotes the basic module in the standard path, $g_k(*)$ denotes the basic module replaced by atrous convolution in the atrous path (k denotes dilated rate), w_1 is weights of the standard path, and w_2 is weights of the atrous path.

$$y = w_1 \cdot f_1(x) + w_2 \cdot g_k(x) \tag{1}$$

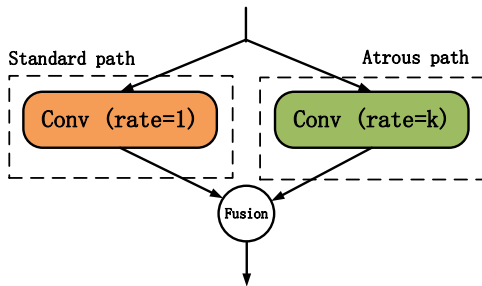


Figure 2. The structure of standard Multi-Receptive Field module. Each Conv represents a basic unit in backbone, such as bottleneck in ResNet. Each path has different receptive field. The output of each path is added by the weight. Each color represents a path.

Multi-Receptive Field Module Lite(MRFM-lite): In order to achieve a trade-off between speed and performance, we explore whether it can capture multi-scale receptive fields without increasing parameters. The two paths of MRFM are exactly the same except for the dilated rate. Now that two paths are identical except for the dilated rate, then we share all the parameters of each path. This method can effectively reduce the number of parameters, but it can still capture the multi-receptive field. Therefore, the model obtained through this structure training will have better per-

formance. The number of parameters decrease, but the computation doesn’t decrease during inference. In order to reduce the computation during inference, thanks to sharing parameters, we could remove atrous path easily, then we fine tune parameters for the better performance. In addition, when we fine tune the parameters, we use a smaller learning rate and fix the batch normalization. So, we call all of these processes Multi-Receptive Field Module Lite (MRFM-lite), illustrated in the Figure 3. In simple terms, the first step is to train the network with the shared parameters dual paths, and the second step is to remove atrous path and fine tune the parameters. MRFM-lite achieves a trade-off between speed and performance.

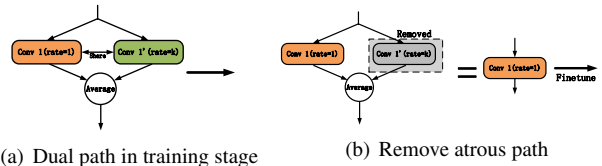


Figure 3. The process of Multi-Receptive Field Module Lite. Each Conv represents a basic unit in backbone, such as bottleneck in ResNet.

In summary, we propose two versions of MRFM. Standard MRFM could replace any basic module to capture multi-receptive field in the backbone. Although introducing parameters, MRFM performs better. MRFM-lite does not increase parameters and computation, but it still can capture multi-receptive field. MRFM and MRFM-lite both can be applied to mainstream backbone, such as ResNet, Xception.

2.2. Edge Aware Loss

By observing the results in the Figure 4, we find that pixels near the edge of an object often tend to be incorrectly classified. So, we propose a new edge aware loss(EAL).

The main idea is that during the training, a pixel close to or on the edge is assigned a weight which incurs a weighted penalty for the classifier. As shown in the Figure 5, the closer the pixel to the edge, the greater the weight. Im-

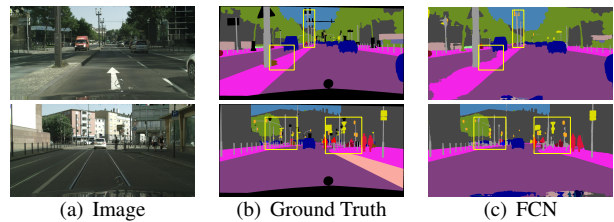


Figure 4. It is difficult to distinguish the boundaries of objects/stuff. Pixels located near the edge of Road and Pole are often incorrectly predicted.

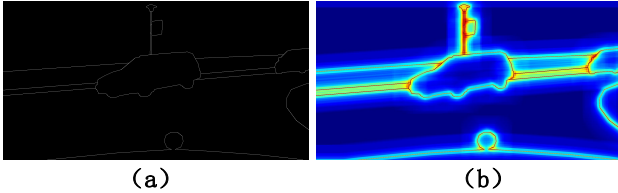


Figure 5. The weight map of edge aware loss. (a) shows the edge detection result on the ground truth. (b) shows the weights map that edge aware loss generates. The closer the edge is, the brighter it will be.

portantly, EAL doesn’t need introduce additional annotated samples. Here is the calculation process for EAL: First, edge is detected on annotated ground truth with Sobel [10], and the edge map is got. Second, to get the weight associated with the pixel’s distance to the edge, we apply a $k \times k$ convolution, which is filled by 1, on the edge map. Third, to prevent the weight from getting too large, set a threshold. The entire calculation process can be expressed in the following Equation 2, where x denotes the ground truth, $C_k(*)$ donates the $k \times k$ convolution filled by 1, $E(*)$ donates the edge detection, $Threshold$ donates max value of the weight map. Finally, we get a weight map which incurs a weighted penalty for classified. This weight map multiplies the output that compute by cross entropy, as shown in Equation 3, where y denotes the outputs of the network, w donates the weight map.

$$w = \min\{C_k(E(x)), Threshold\} \quad (2)$$

$$L = SoftmaxLoss(y; w) \quad (3)$$

2.3. Network Architecture

With the multi-receptive field module, we propose a *Multi-Receptive Field Network* architecture based on Xception modified by [7] as illustrated in Figure 6 . Here we think of [7] as a powerful backbone. Given an input image, we use Xception model with the dilated network strategy. Meanwhile, replace the basic module in middle flow and exit flow’s block1 with MRFM. In addition, the final feature map spatial size is 1/16 of the input image. Then ASPP and Decoder, which are same as [7], are also employed. At last, we employ EAL to compute loss.

3. Experiments

We evaluate our approach on two public and widely used semantic image segmentation datasets, Cityscapes [9] and Pascal VOC2012 [11]. We first report the implementation details. Then we perform a series of ablation experiments on Cityscapes, and analyze the results in detail. Finally, we

report our results on Pascal VOC2012 compared with other state-of-the-art methods.

3.1. Implementation Details

Our proposed network is based on the Xception modified by [7] pretrained on ImageNet [19]. In order to better demonstrate the improvement of the network performance of the module, our work is based on FCN.

Training: Following previous work [5], we use the “poly” learning rate policy where the base learning rate is multiplied by $(1 - \frac{iter}{iter_{max}})^{power}$. The initial learning rate is set to 0.1, and power is set to 0.9. We train the network using mini-bath stochastic gradient descent(SGD) [19]. Momentum and weight decay coefficients are set to 0.9 and 0.0004 respectively. The size of mini-batch is set to 12. We employ crop size of 513 during Cityscapes and Pascal VOC2012 dataset.

Data augmentation: Following [6], we use mean subtraction, apply data augmentation by randomly scaling the input images with 7 scales {0.5, 0.75, 1, 1.25, 1.5, 1.75, 2.0} and randomly left-right flipping during training.

3.2. Cityscapes Dataset

Dataset and Evaluation Metrics: Cityscapes is a large and famous city street scene semantic segmentation dataset [9]. 19 classes of which 30 classes of this dataset are considered for training and evaluation. Each image has a high resolution 2048×1024 pixels. Cityscapes has 5,000 images taken from 50 different cities which are all fine annotation. In these 5,000 images, there are 2,979 images for training, 500 images for validation and 1,525 images for testing. There are also 19,998 images with coarse annotation. Cityscapes In the same image, cityscapes have many scale objects, such as road, sky, vehicles, persons and so on. In the same category, persons, cars, sky and so on also have a lot of scales. So cityscapes is a dataset that is extremely sensitive to the scale. In this challenging dataset, our method outperforms previous methods again. For evaluation, *mean class-wise intersection over union* (mIoU) is used.

Ablation Study for MRFM in Xception: In order to evaluate the improvement of MRFM and MRFM-lite, we carry out some experiments. As listed in the Table 1, without more parameters, MRFM-lite-2 significantly improves the segmentation performance over the Xception41-baseline model by 2.7%. MRFM-lite is trained in two stages, and we also provide the results of two stages. Compared with baseline, MRFM-lite-2(DP) get a 2.2% promotion. Compared with MRFM-lite-2(DP), MRFM-lite-2(OP), which is fine tuned with one path, get a 0.5% promotion. Particularly, when we fine tune MRFM-lite, we set the learning rate to 0.01 and fix batch normalization. We

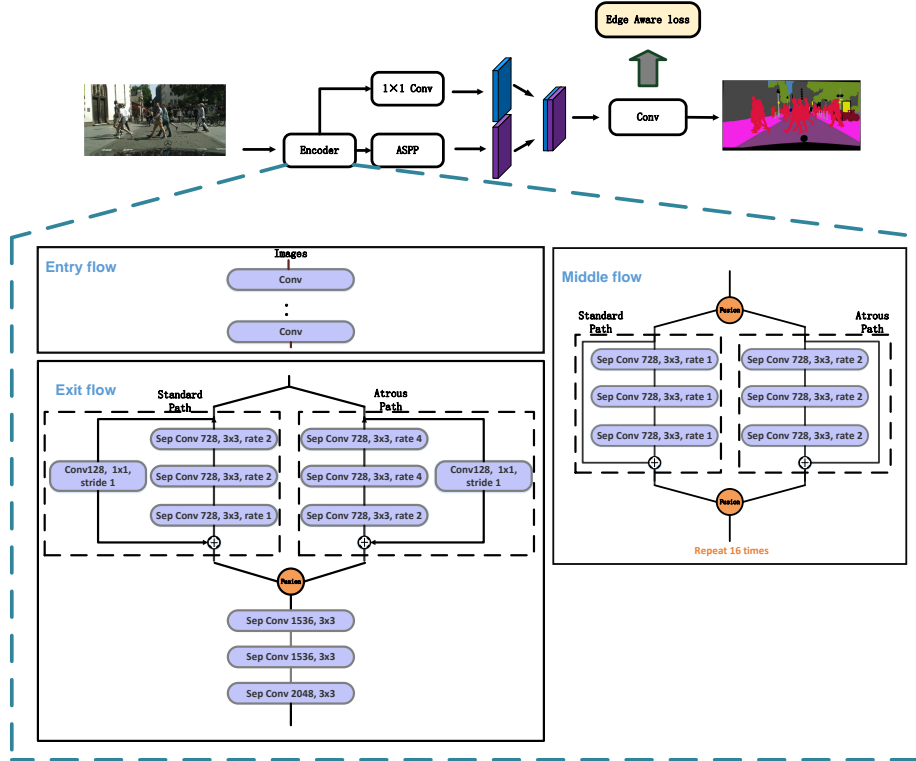


Figure 6. Overview of Multi Receptive Field Network Architecture.

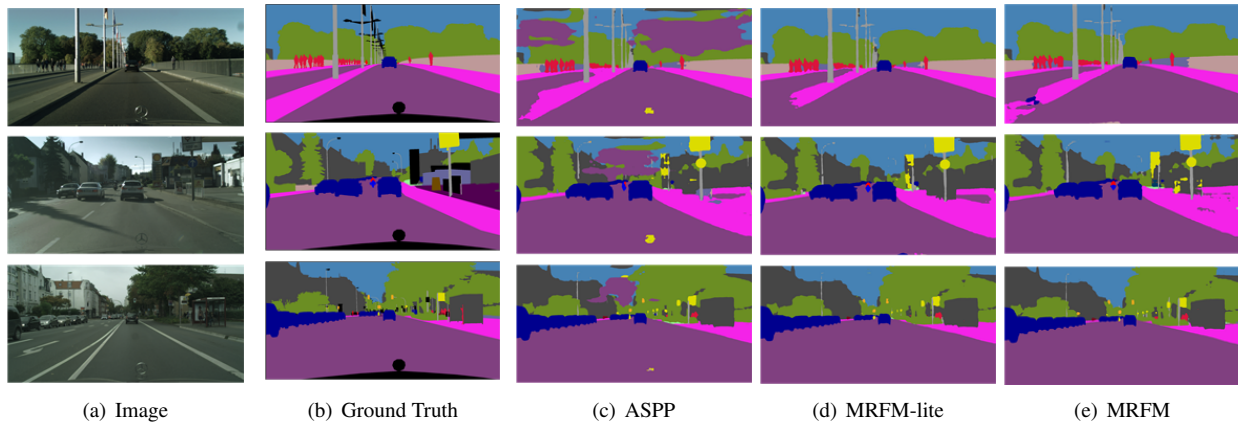


Figure 7. Visual improvements on Cityscapes. Based on FCN, MRFM and MRFM-lite produces more accurate and detailed results.

find it is important to fix batch normalization. It is worth noting that compared with Xception41, MRFM-lite has the same structure, the same speed and higher performance. In order to fairly compare the performance of MRFM under the similar model capacity, we also give the baseline performance of Xception65 and Xception71. With the increase of model capacity, the performance of the model has been improved, but MRFM is still better than Xception71, which has the largest model capacity. Specially, with MRFM-4,

the network is the best, which increases 3.4% that is compared with Xception41, and increases 1.9% that is compared with Xception71! In addition, compared with ASPP that is famous method to capture multi-scale receptive field, MRFM-lite is slightly better than ASPP without introducing more parameters and time, and MRFM also has a great improvement over ASPP.

The receptive fields of both paths interact with each other. So MRFM-lite-2 is better than MRFM-lite-4. How-

Method	mIoU(%)
Xception41-Baseline	72.5
Xception65-Baseline	73.1
Xception71-Baseline	74.0
Xception41+ASPP	75.0
Xception41+MRFM-lite-2(DP)	74.7
Xception41+MRFM-lite-2(OP)	75.2
Xception41+MRFM-lite-4(OP)	72.2
Xception41+MRFM-lite-4(DP)	72.4
Xception41+MRFM-2	75.7
Xception41+MRFM-4	75.9
Xception41+MRFM-8	72.3
Xception41+MRFM-4(Exit flow)	74.3
Xception41+MRFM-4(Middle flow)	74.2

Table 1. Investigation of MRFM with different settings. Baseline is Xception41-based FCN in which output stride is 16. MRFM-(*) present dilated rate in the atrous path. DP present dual path of MRFM-lite in training stage. OP present MRFM-lite is fine tuned with one path. MRFM(Exit flow) is represented as replacing the exit flow module with MRFM module. MRFM(Middle flow) is represented as replacing the middle flow module with MRFM module. To simplify the presentation, MRFM without special instructions replaces the basic module in middle flow and exit flow.

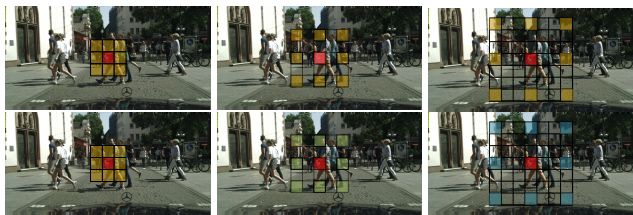


Figure 8. Different receptive field. The same color represents the same parameters. The top row shows MRFM-lite. The bottom row shows standard MRFM. Each row shows different MRFM’s receptive field. As shown in each row, receptive field becomes large different by increasing dilation rate.

ever, in the standard MRFM, MRFM-4 is better than MRFM-2, but MRFM-8 is very terrible. As shown in Figure 8, with the increase of the dilated rate, the information of different receptive field becomes more different. So, if the receptive field of each path is much different, it is harmful. In addition, the convolution parameters of the two paths in MRFM-lite are more relevant than those of the two paths in MRFM. Therefore, the difference of dilated rate that is in the each path of MRFM can be greater. It is precisely because the receptive fields are not mutually constrained that MRFM is 0.7% higher than MRFM-lite.

Comparing the performance differences of different parts using MRFM. MRFM in exit flow and MRFM in middle flow both bring about improvement than baseline. MRFM in both middle flow and exit flow is better than

MRFM in one flow.

At last, all of experiments show that we use MRFM when we need higher accuracy and MRFM-lite when we need trade-off speed and accuracy. Both versions of MRFM can improve the basic performance of the model.

Ablation Study for MRFM in ResNet: In order to demonstrate the general of MRFM, we also product some experiments on ResNet50. As illustrated in the Table 2, all of settings are better than baseline. MRFM-4 has increased 4.8% over the baseline network. Compared with FCN, MRFM-lite-2 has improved 3.5% without any more parameters. Compared with MRFM-lite-2(DP), MRFM-lite-2(OP) has improved 1.8% . These experiments show MRFM and MRFM-lite could extend to other backbone easily. In addition, compared with ASPP, MRFM and MRFM-lite are also standout. Through Xception and Resnet experiments, we can boldly speculate that MRFM can be applied to other backbone.

Method	mIoU(%)
ResNet50-Baseline	65.9
ResNet50+ASPP	69.3
ResNet50+MRFM-lite-2(DP)	67.2
ResNet50+MRFM-lite-2(OP)	69.4
ResNet50+MRFM-4	70.7

Table 2. In order to demonstrate the generalization ability of the MRFM better, ResNet experiments are conduct

Ablation Study for Receptive Field: As illustrated in the Table 3, some experiments are organized to represent the effects of different receptive field methods. InceptionV4 [31] uses a lot of pooling operations, and the operation of pooling will result in the loss of details. So the result of InceptionV4 [31] is very poor. ResNet50-DCN [42] applies deformable convolution in the stage2, stage3 and stage4. DCN [42] effectively improved performance by 2.6%. However, MRFM-lite is still 0.9% better than ResNet50-DCN, and MRFM is still 2.2% better than ResNet50-DCN. We think that DCN is an implicit way to learn multi-scale information, but MRFM and MRFM-lite are an explicit way to learn multi-scale information, so MRFM and MRFM-lite perform better.

Method	mIoU(%)
InceptionV4	51.5
ResNet50	65.9
ResNet50-DCN	68.5
ResNet50+MRFM-lite-2	69.4
ResNet50+MRFM-4	70.7

Table 3. Much work has been done to obtain different scales of the receptive field. The experiments are conduct. DCN present the deformable convolution [42]. The output stride of InceptionV4 [31] is 16.

Method	mIoU(%)
Cross Entropy	72.5
Edge Branch	72.7
OHEM [30, 34]	73.0
Lovas Loss [2]	72.8
EAL	74.1

Table 4. Different loss functions brings different improvement. To prove EAL’s more efficient, some experiments are conduct.

Method	k	m	mIoU(%)
Baseline			78.1
EAL	5	3	78.6
EAL	7	3	78.5

Table 5. In order to demonstrate the influence of the different hyperparameters, experiments are conduct. Except that backbone is replaced with Xception41, the rest of baseline is the same as deeplabv3+.

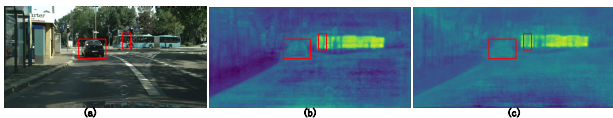


Figure 9. Visual improvements with EAL. (a) shows RGB image; (b) shows feature map with EAL; (c) shows feature map without EAL.

Ablation Study for Edge Aware Loss: The introduced EAL helps to detect object contour while not affecting learning process in the main master. In particular, as we have mentioned before, EAL doesn’t require additional annotations. In the Table 4, compared with baseline, EAL brings 1.6% improvement. DFN [37] proposed the multi task methods, including edge segmentation task and semantic segmentation task. So EAL is also compared with edge branch method. When adding edge branch, the model shares the backbone, and each task has its own two convolution operations. As illustrated in the Table 4, the result is almost similar with Cross Entropy. Because different tasks have its own unique parameters, It’s hard for edge branch to influence the main task. In addition, edges can be considered as difficult samples, so we also compare OHEM [30, 34]. Compared with OHEM [30, 34], EAL brings 1.1% improvement. Lovas loss solves the gap between loss function and mIoU in semantic segmentation. To better illustrate the effectiveness of EAL, we also compared the difference with Lovas loss. Compared with Lovas loss, EAL brings 1.3% improvement. In the Figure 9, with EAL, edges can be clearly seen. When using EAL, two hyperparameters are added. One is k, which determines the longest distance of the edge, and the other is m, which determines the maximum weight. In the Table 5, it shows that EAL can improve steadily under different hyperparameters.

Framework Details: In order to show the effect of each

Baseline	ASPP	MRFM-lite-2	MRFM-4	EAL	mIoU
Xception41					72.5
Xception41		✓			75.2
Xception41			✓		75.9
Xception41	✓				75.0
Xception41	✓	✓			76.2
Xception41	✓	✓		✓	76.3
Xception41	✓		✓		76.7
Xception41	✓		✓	✓	77.7
Xception65+Decoder	✓				78.4
Xception65+Decoder	✓		✓		79.7
Xception65+Decoder	✓		✓	✓	80.2

Table 6. Ablation Study for the each module.

module in our framework and show the continuous improvement with our methods, we conducted some experiments, illustrated in the Table 6. Based on FCN (Xception41) and deeplabv2 (Xception41+ASPP) [5], MRFM, MRFM-lite and EAL could bring improvement. Based on powerful deeplabv3+ (Xception65) [7], our MRFM could bring 1.4%. It is noteworthy that MRFM has continued to improve with ASPP. Although MRFM has acquired multi-scale information in backbone, as shown in the Table 6, ASPP can still obtain multi-scale information. Since ASPP is located behind backbone and is closer to output, it is meaningful to obtain multi-scale in any part of the network. We can also see that MRFM does improve the performance of backbone, so MRFM does have the prospect of improving segmentation baseline. In addition, we speculate that replacing ASPP with better modules will lead to better results, such as replacing DPC [4], DRN [43], etc. The highest performance MRFM can be improved by 0.5% with EAL and get a mIoU of 80.2% on the validation. At last, we get the best performance model, which contains deeplabv3+, MRFM-4 and EAL.

Ablation Study for different scale testing: In order to show more clearly that MRFM performs better than single-scale model in different scales, we organized a group of experiments. Image sent to the network are scaled to form different scales. Illustrated in the Tabel 7, the results of each scale are more better than the results of single-scale model. Moreover, by calculating the standard deviation, it is found that the results fluctuate less in each scale, so it can be proved that MRFM is robust for multi-scale.

Method	0.5s	0.75s	1.0s	1.25s	1.5s	1.75s	2.0s	STD
Baseline	72.7	76.8	78.4	78.8	78.6	77.9	76.6	1.97
MRFM	75.1	78.4	79.8	80.3	80.0	79.6	78.1	1.68

Table 7. Each column represents how many times the input image is the original image. The results show that MRFM is superior to single-scale model in different scales. The baseline is same as Deeplabv3+.

Comparing with State-of-the-art: We further compare our method with the state-of-the-art methods on the Cityscapes test set. For maximum performance, we

Methods	road	swalk	build.	wall	fence	pole	tlight	sign	veg	terrain	sky	person	rider	car	truck	bus	train	mbike	bike	IoU
DUC [33]	98.5	85.9	93.2	57.7	61.1	67.2	73.7	78.0	93.4	72.3	95.4	85.9	70.5	95.9	76.1	90.6	83.7	67.4	75.7	80.1
DFN [37]	98.6	85.9	93.2	59.6	61.0	66.6	73.2	78.2	93.5	71.6	95.5	86.5	70.5	96.1	77.1	89.9	84.7	68.2	76.5	80.3
ResNet38 [34]	98.7	86.9	93.3	60.4	62.9	67.6	75.0	78.7	93.7	73.7	95.5	86.8	71.1	96.1	75.2	87.6	81.9	69.8	76.7	80.6
PSPNet [41]	98.7	86.9	93.5	58.4	63.7	67.7	76.1	80.5	93.6	72.2	95.3	86.8	71.9	96.2	77.7	91.5	83.6	70.8	77.5	81.2
DeepLabv3 [6]	98.6	86.2	93.5	55.2	63.2	70.0	77.1	81.3	93.8	72.3	95.9	87.6	73.4	96.3	75.1	90.4	85.1	72.1	78.3	81.3
AdapNet++ [32]	98.6	86.2	93.3	57.8	62.0	67.3	75.0	79.6	93.6	72.3	95.3	86.4	72.2	96.2	81.5	92.4	88.0	71.2	76.6	81.3
Mapillary [27]	98.4	85.0	93.6	61.7	63.9	67.7	77.4	80.8	93.7	71.9	95.6	86.7	72.8	95.7	79.9	93.1	89.7	72.6	78.2	82.0
DeepLabv3+ [7]	98.7	87.0	93.9	59.5	63.7	71.4	78.2	82.2	94.0	73.0	95.8	88.0	73.3	96.4	78.0	90.9	83.9	73.8	78.9	82.1
AutoDeepLab [24]	98.8	87.6	93.8	61.4	64.4	71.2	77.6	80.9	94.1	72.7	96.0	87.8	72.8	96.5	78.2	90.9	88.4	69.0	77.6	82.1
DPC [4]	98.7	87.1	93.8	57.7	63.5	71.0	78.0	82.1	94.0	73.3	95.4	88.2	74.5	96.5	81.2	93.3	89.0	74.1	79.0	82.7
DRN [43]	98.8	87.7	94.0	65.1	64.2	70.1	77.4	81.6	93.9	73.5	95.8	88.0	74.9	96.5	80.8	92.1	88.5	72.1	78.8	82.8
Ours	98.8	88.0	94.2	63.8	64.7	72.3	78.3	81.8	94.2	73.9	95.7	88.3	74.6	96.4	79.5	92.2	88.1	72.8	78.6	83.0

Table 8. Results on Cityscapes testing set. Methods are trained using both fine and coarse data. The best entry in each columns is marked in gray color.(Note: the methods that only use cityscapes dataset are included.)

Method	aero	bike	bird	boat	bottle	bus	car	cat	chair	cow	table	dog	horse	mbike	person	plant	sheep	sofa	train	tv	mIoU
RefineNet [21]	95.0	73.2	93.5	78.1	84.8	95.6	89.8	94.1	43.7	92.0	77.2	90.8	93.4	88.6	88.1	70.1	92.9	64.3	87.7	78.8	84.2
ResNet38 [34]	96.2	75.2	95.4	74.4	81.7	93.7	89.9	92.5	48.2	92.0	79.9	90.1	95.5	91.8	91.2	73.0	90.5	65.4	88.7	80.6	84.9
PSPNet [41]	95.8	72.7	95.0	78.9	84.4	94.7	92.0	95.7	43.1	91.0	80.3	91.3	96.3	92.3	90.1	71.5	94.4	66.9	88.8	82.0	85.4
DeepLabv3 [6]	96.4	76.6	92.7	77.8	87.6	96.7	90.2	95.4	47.5	93.4	76.3	91.4	97.2	91.0	92.1	71.3	90.9	68.9	90.8	79.3	85.7
EncNet [39]	95.3	76.9	94.2	80.2	85.3	96.5	90.8	96.3	47.9	93.9	80.0	92.4	96.6	90.5	91.5	70.9	93.6	66.5	87.7	80.8	85.9
DFN [37]	96.4	78.6	95.5	79.1	86.4	97.1	91.4	95.0	47.7	92.9	77.2	91.0	96.7	92.2	91.7	76.5	93.1	64.4	88.3	81.2	86.2
SDN [12]	96.9	78.6	96.0	79.6	84.1	97.1	91.9	96.6	48.5	94.3	78.9	93.6	95.5	92.1	91.1	75.0	93.8	64.8	89.0	84.6	86.6
DeepLabv3+ [7]	97.0	77.1	97.1	79.3	89.3	97.4	93.2	96.6	56.9	95.0	79.2	93.1	97.0	94.0	92.8	71.3	92.9	72.4	91.0	84.9	87.8
ExFuse [40]	96.8	80.3	97.0	82.5	87.8	96.3	92.6	96.4	53.3	94.3	78.4	94.1	94.9	91.6	92.3	81.7	94.8	70.3	90.1	83.8	87.9
MSCI [20]	96.8	76.8	97.0	80.6	89.3	97.4	93.8	97.1	56.7	94.3	78.3	93.5	97.1	94.0	92.8	72.3	92.6	73.6	90.8	85.4	88.0
Ours	97.1	78.6	97.1	80.6	89.7	97.3	93.6	96.7	59.0	95.4	81.1	93.2	97.5	94.2	92.9	72.3	93.1	74.2	91.0	85.0	88.4

Table 9. Per-class results on PASCAL VOC2012 testing set. Methods are all pre-trained on MS-COCO. The best entry in each columns is marked in gray color.(Note: the methods that use the public dataset are included.)



Figure 10. Visualization results on Cityscapes test set.

use the best structure in the Table 6, which consists of DeepLabV3+(Xception65), MRFM and EAL. In particular, we use only fine-coarse data training networks, and submit our results to the official evaluation server. Results are shown in Table 8. The result shows that our method is better than previous method in some categories, such as building, pole, traffic light, terrain, person. Because these classes have diverse scales.

3.3. Pascal VOC2012 Dataset

Pascal VOC2012: The Pascal VOC2012 is well-known object segmentation dataset that includes 20 object cate-

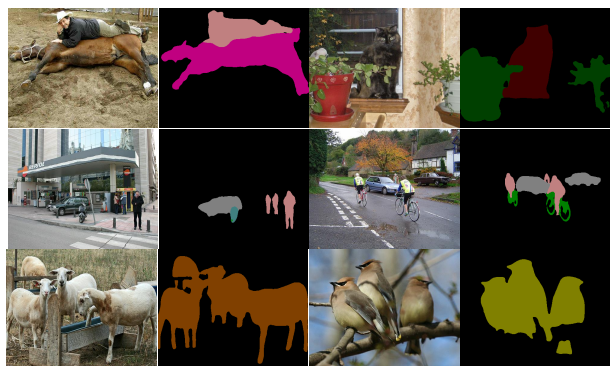


Figure 11. Visualization results on Pascal VOC2012 test set.

gories and one background categories. There are 1,464 images for training, 1,449 images for evaluation and 1,456 images for testing. According to the common convention, we augment the training set by additional annotated VOC images provided in [14] and the MS COCO dataset [23].

We follow the same strategy to train our model on the Pascal VOC2012 dataset. The model used in Pascal VOC dataset is the same as the model used in cityscapes dataset. Table 9 indicates the experiment results on Pascal VOC2012 testing set. Our proposed network achieves 88.4% mIoU, outperforming other previous state-of-the-art methods. Compared with [7], it increases 0.6%. The results

show that our method is better than the previous method for the variable scales object, such as aeroplane, bird, cow, horse, person.

4. Conclusion

In this paper, we have presented a Multi-Receptive Field Network for semantic segmentation. In order to capture multi-receptive field, the Multi-Receptive Field Module is proposed as a general module. Furthermore, MRFM-lite could achieve the trade-off between performance and speed. You can use different versions of the MRFM according to your needs. We have also provided an Edge Aware Loss which is effective in distinguishing the boundaries of object/stuff. At last, We hope our method could help all tasks of semantic segmentation improve the overall baseline.

References

- [1] Vijay Badrinarayanan, Alex Kendall, and Roberto Cipolla. Segnet: A deep convolutional encoder-decoder architecture for image segmentation. *arXiv preprint arXiv:1511.00561*, 2015. 2
- [2] Maxim Berman, Amal Rannen Triki, and Matthew B Blaschko. The lovász-softmax loss: A tractable surrogate for the optimization of the intersection-over-union measure in neural networks. In *Proceedings of the IEEE Conference on Computer Vision and Pattern Recognition*, pages 4413–4421, 2018. 7
- [3] Holger Caesar, Jasper Uijlings, and Vittorio Ferrari. Coco-stuff: Thing and stuff classes in context. *CoRR, abs/1612.03716*, 5:8, 2016. 1
- [4] Liang-Chieh Chen, Maxwell D Collins, Yukun Zhu, George Papandreou, Barret Zoph, Florian Schroff, Hartwig Adam, and Jonathon Shlens. Searching for efficient multi-scale architectures for dense image prediction. *arXiv preprint arXiv:1809.04184*, 2018. 7, 8
- [5] Liang-Chieh Chen, George Papandreou, Iasonas Kokkinos, Kevin Murphy, and Alan L Yuille. Deeplab: Semantic image segmentation with deep convolutional nets, atrous convolution, and fully connected crfs. *IEEE transactions on pattern analysis and machine intelligence*, 40(4):834–848, 2017. 2, 4, 7
- [6] Liang Chieh Chen, George Papandreou, Florian Schroff, and Hartwig Adam. Rethinking atrous convolution for semantic image segmentation. *arXiv:1706.05587*, 2017. 1, 4, 8
- [7] Liang Chieh Chen, Yukun Zhu, George Papandreou, Florian Schroff, and Hartwig Adam. Encoder-decoder with atrous separable convolution for semantic image segmentation. *arXiv:1802.02611v3*, 2018. 4, 7, 8
- [8] François Chollet. Xception: Deep learning with depthwise separable convolutions. *arXiv preprint*, pages 1610–02357, 2017. 3
- [9] Marius Cordts, Mohamed Omran, Sebastian Ramos, Timo Rehfeld, Markus Enzweiler, Rodrigo Benenson, Uwe Franke, Stefan Roth, and Bernt Schiele. The cityscapes dataset for semantic urban scene understanding. In *Proceedings of the IEEE conference on computer vision and pattern recognition*, pages 3213–3223, 2016. 1, 2, 4
- [10] Richard O Duda, Peter E Hart, et al. *Pattern classification and scene analysis*, volume 3. Wiley New York, 1973. 4
- [11] M Everingham, L Van Gool, CKI Williams, J Winn, and A Zisserman. The pascal visual object classes challenge 2012 results. In *See http://www.pascal-network.org/challenges/VOC/voc2012/workshop/index.html*, volume 5, 2012. 1, 2, 4
- [12] Jun Fu, Jing Liu, Yuhang Wang, and Hanqing Lu. Stacked deconvolutional network for semantic segmentation. *arXiv preprint arXiv:1708.04943*, 2017. 8
- [13] Stephen Gould, Richard Fulton, and Daphne Koller. Decomposing a scene into geometric and semantically consistent regions. In *Computer Vision, 2009 IEEE 12th International Conference on*, pages 1–8. IEEE, 2009. 1
- [14] Bharath Hariharan, Pablo Arbeláez, Lubomir Bourdev, Subhransu Maji, and Jitendra Malik. Semantic contours from inverse detectors. In *2011 International Conference on Computer Vision*, pages 991–998. IEEE, 2011. 1, 8
- [15] Kaiming He, Xiangyu Zhang, Shaoqing Ren, and Jian Sun. Deep residual learning for image recognition. In *Proceedings of the IEEE conference on computer vision and pattern recognition*, pages 770–778, 2016. 1, 2, 3
- [16] Xuming He, Richard S Zemel, and Miguel Á Carreira-Perpiñán. Multiscale conditional random fields for image labeling. In *Computer vision and pattern recognition, 2004. CVPR 2004. Proceedings of the 2004 IEEE computer society conference on*, volume 2, pages II–II. IEEE, 2004. 1
- [17] Gao Huang, Zhuang Liu, Laurens Van Der Maaten, and Kilian Q Weinberger. Densely connected convolutional networks. In *Proceedings of the IEEE conference on computer vision and pattern recognition*, pages 4700–4708, 2017. 2
- [18] Pushmeet Kohli, Philip HS Torr, et al. Robust higher order potentials for enforcing label consistency. *International Journal of Computer Vision*, 82(3):302–324, 2009. 1
- [19] Alex Krizhevsky, Ilya Sutskever, and Geoffrey E. Hinton. Imagenet classification with deep convolutional neural networks. In *International Conference on Neural Information Processing Systems*, pages 1097–1105, 2012. 4
- [20] Di Lin, Yuanfeng Ji, Dani Lischinski, Daniel Cohen-Or, and Hui Huang. Multi-scale context intertwining for semantic segmentation. In *Proceedings of the European Conference on Computer Vision (ECCV)*, pages 603–619, 2018. 2, 8
- [21] Guosheng Lin, Anton Milan, Chunhua Shen, and Ian Reid. Refinenet: Multi-path refinement networks for high-resolution semantic segmentation. In *Proceedings of the IEEE conference on computer vision and pattern recognition*, pages 1925–1934, 2017. 2, 8
- [22] Guosheng Lin, Chunhua Shen, Anton Van Den Hengel, and Ian Reid. Efficient piecewise training of deep structured models for semantic segmentation. In *Proceedings of the IEEE conference on computer vision and pattern recognition*, pages 3194–3203, 2016. 1
- [23] Tsung-Yi Lin, Michael Maire, Serge Belongie, James Hays, Pietro Perona, Deva Ramanan, Piotr Dollár, and C Lawrence

- Zitnick. Microsoft coco: Common objects in context. In *European conference on computer vision*, pages 740–755. Springer, 2014. 1, 8
- [24] Chenxi Liu, Liang-Chieh Chen, Florian Schroff, Hartwig Adam, Wei Hua, Alan L Yuille, and Li Fei-Fei. Auto-deeplab: Hierarchical neural architecture search for semantic image segmentation. In *Proceedings of the IEEE conference on computer vision and pattern recognition*, pages 82–92, 2019. 8
- [25] Jonathan Long, Evan Shelhamer, and Trevor Darrell. Fully convolutional networks for semantic segmentation. In *Proceedings of the IEEE conference on computer vision and pattern recognition*, pages 3431–3440, 2015. 1, 2
- [26] Olaf Ronneberger, Philipp Fischer, and Thomas Brox. U-net: Convolutional networks for biomedical image segmentation. In *International Conference on Medical image computing and computer-assisted intervention*, pages 234–241. Springer, 2015. 2
- [27] Samuel Rota Bulò, Lorenzo Porzi, and Peter Kotschieder. In-place activated batchnorm for memory-optimized training of dnns. In *Proceedings of the IEEE Conference on Computer Vision and Pattern Recognition*, pages 5639–5647, 2018. 8
- [28] Chris Russell, Pushmeet Kohli, Philip HS Torr, et al. Associative hierarchical crfs for object class image segmentation. In *Computer Vision, 2009 IEEE 12th International Conference on*, pages 739–746. IEEE, 2009. 1
- [29] Jamie Shotton, John Winn, Carsten Rother, and Antonio Criminisi. Textonboost for image understanding: Multi-class object recognition and segmentation by jointly modeling texture, layout, and context. *International Journal of Computer Vision*, 81(1):2–23, 2009. 1
- [30] Abhinav Shrivastava, Abhinav Gupta, and Ross Girshick. Training region-based object detectors with online hard example mining. In *IEEE Conference on Computer Vision & Pattern Recognition*, 2016. 7
- [31] Christian Szegedy, Sergey Ioffe, Vincent Vanhoucke, and Alexander A Alemi. Inception-v4, inception-resnet and the impact of residual connections on learning. In *Thirty-First AAAI Conference on Artificial Intelligence*, 2017. 6
- [32] Abhinav Valada, Rohit Mohan, and Wolfram Burgard. Self-supervised model adaptation for multimodal semantic segmentation. *International Journal of Computer Vision*, pages 1–47, 2019. 8
- [33] Panqu Wang, Pengfei Chen, Ye Yuan, Ding Liu, Zehua Huang, Xiaodi Hou, and Garrison Cottrell. Understanding convolution for semantic segmentation. In *2018 IEEE winter conference on applications of computer vision (WACV)*, pages 1451–1460. IEEE, 2018. 8
- [34] Zifeng Wu, Chunhua Shen, and Anton Van Den Hengel. Wider or deeper: Revisiting the resnet model for visual recognition. *Pattern Recognition*, 90:119–133, 2019. 7, 8
- [35] Maoke Yang, Kun Yu, Chi Zhang, Zhiwei Li, and Kuiyuan Yang. Denseaspp for semantic segmentation in street scenes. In *Proceedings of the IEEE Conference on Computer Vision and Pattern Recognition*, pages 3684–3692, 2018. 2
- [36] Jian Yao, Sanja Fidler, and Raquel Urtasun. Describing the scene as a whole: Joint object detection, scene classification and semantic segmentation. In *Computer Vision and Pattern Recognition (CVPR), 2012 IEEE Conference on*, pages 702–709. IEEE, 2012. 1
- [37] Changqian Yu, Jingbo Wang, Chao Peng, Changxin Gao, Gang Yu, and Nong Sang. Learning a discriminative feature network for semantic segmentation. *arXiv preprint arXiv:1804.09337*, 2018. 2, 7, 8
- [38] Fisher Yu and Vladlen Koltun. Multi-scale context aggregation by dilated convolutions. *arXiv preprint arXiv:1511.07122*, 2015. 2
- [39] Hang Zhang, Kristin Dana, Jianping Shi, Zhongyue Zhang, Xiaoang Wang, Amrbrish Tyagi, and Amit Agrawal. Context encoding for semantic segmentation. In *The IEEE Conference on Computer Vision and Pattern Recognition (CVPR)*, 2018. 8
- [40] Zhenli Zhang, Xiangyu Zhang, Chao Peng, Dazhi Cheng, and Jian Sun. Exfuse: Enhancing feature fusion for semantic segmentation. *arXiv preprint arXiv:1804.03821*, 2018. 8
- [41] Hengshuang Zhao, Jianping Shi, Xiaojuan Qi, Xiaoang Wang, and Jiaya Jia. Pyramid scene parsing network. In *Proceedings of the IEEE conference on computer vision and pattern recognition*, pages 2881–2890, 2017. 1, 2, 8
- [42] Xizhou Zhu, Han Hu, Stephen Lin, and Jifeng Dai. Deformable convnets v2: More deformable, better results. In *Proceedings of the IEEE Conference on Computer Vision and Pattern Recognition*, pages 9308–9316, 2019. 6
- [43] Yueqing Zhuang, Fan Yang, Li Tao, Cong Ma, Ziwei Zhang, Yuan Li, Huizhu Jia, Xiaodong Xie, and Wen Gao. Dense relation network: Learning consistent and context-aware representation for semantic image segmentation. In *2018 25th IEEE International Conference on Image Processing (ICIP)*, pages 3698–3702. IEEE, 2018. 7, 8
- [44] Roland S Zimmermann and Julien N Siems. Faster training of mask r-cnn by focusing on instance boundaries. *arXiv preprint arXiv:1809.07069*, 2018. 2